FORM TI-12
2/99

B-T-3238

The Development and Testing of Emissivity Enhancement Coatings for Thermophotovoltaic (TPV) Radiator Applications

B.V. Cockeram, D.P. Measures, and A.J. Mueller

USDOE contract No. DE-AC11-98PN38206

BETTIS ATOMIC POWER LABORATORY WEST MIFFLIN, PENNSYLVANIA 15122-0079

Operated for the U.S. Department of Energy
by Bechtel Bettis, Inc.

DISCLAIMER

The Development and Testing of Emissivity Enhancement Coatings for Thermophotovoltaic (TPV) Radiator Applications

B.V. Cockeram, D.P. Measures, and A.J. Mueller

Bettis Atomic Power Laboratory, P.O. Box 79, West Mifflin, PA 15122-0079.

Abstract

One requirement of a TPV radiator is to efficiently emit photons at high temperatures to TPV cells for conversion to electric power. Since many candidate radiator materials with adequate structural properties display low emissivity, coatings or other surface modifications are required for enhancement of emissivity. Coatings or other surface modifications using vacuum plasma spray (ZrO_2 + 18% TiO_2 + 10% Y_2O_3, Cr_2O_3, ZrC, Fe_2TiO_5, $ZrTiO_4$, ZrO_2 + 8% Y_2O_3 + 2% HfO_2, TiC, TiC + 5% Al_2O_3 + 5% TiO_2, ZrB_2, ZrB_2 + 10% $MoSi_2$, and Al_2O_3 + 5% TiO_2), arc texturing (carbon and SiC electrodes), slurry fusion (SiO_2 + C), and chemical vapor deposition (rhenium) have been evaluated as means of increasing emissivities of several structural alloys including refractory metals and nickel-base materials. Characterization and emissivity testing of these surfaces in the as-deposited condition and after a 500 hour vacuum anneal are used to evaluate coating performance. Thermal cycling tests were also completed. Six plasma sprayed coatings and one textured surface demonstrated adequate thermal stability and emittance values of 0.8 or greater. Promising attributes of modified surfaces are identified.

1. Introduction

An important component of a thermophotovoltaic (TPV) power generation system is the radiator, which serves to emit infrared (IR) photons from its surface to the TPV cells for conversion to electrical power. A relative measure of the efficiency of photon radiation from a surface is emissivity, with a value of 1.0 being a maximum and representing a perfect black body radiator. Many structural metals suitable for TPV radiator applications have a desirable balance of high-temperature strength and low-temperature ductility, but are limited by a relatively low emissivity (~0.1-0.4).

Two fundamental approaches have been taken to enhance the emissivity of candidate structural materials: (1) application of a coating material that possesses high emissivity and (2) surface modification of the radiator materials to create a rough surface texture with high aspect ratio features (height to width ratio > 5:1) that serve as individual black-bodies. Surface modification approaches being evaluated include atomic oxygen beam texturing, application of rhenium whiskers by chemical vapor deposition (CVD), and laser ablation. Surface modification approaches are potentially attractive because coating/substrate interactions are not an issue. Emissivity enhancement coatings are an attractive approach because these layers could also serve as a protective barrier for the structural alloy, limiting oxidation in accident conditions where air and/or water exposure could occur. Arc texturing using carbon and silicon carbide (SiC) electrodes, thermal spray coatings, and fused silica - carbon (SiO_2 - C) coatings are some of the coating candidates evaluated.

The coatings/surface modifications were characterized in the as-received and post-anneal condition and subjected to thermal cycling to evaluate thermal stability. Total hemispherical emittance in the as-received and post-anneal condition was determined. The test results are discussed and promising candidates are identified.

2. Materials, Coatings, and Procedures

The coatings and/or surface modifications were applied to discs (2.54 cm diameter by 0.15 cm thick with surface roughness of $R_a < 8$ μ-inch) of the following materials: (1) arc cast or powder metallurgy, commercially pure (CP) molybdenum, per ASTM B387-90 Type 361 SR, cleaned in a solution of $HNO_3 + H_2SO_4 + HF$, (2) CP electron-beam melted niobium, per ASTM B392-89 Type 2, cleaned in a solution of 60% water + 30% HNO_3 + 10% HF, and (3) a high strength nickel-base alloy, Haynes 230 cleaned in water.

Ten different Vacuum Plasma Spray (VPS) coatings were deposited on molybdenum, niobium, and Haynes 230 by the Thermal Spray Laboratory at the State University of New York at Stony Brook (SUNY), see Table I.

The coatings were deposited in 2 layers to a total nominal coating thickness of 50-75 μm on one side of the coupons. The layer consisted of: (1) a 25 μm thick bond coat consisting of a 50/50 mixture of substrate powder (molybdenum, niobium, or Haynes 230) and coating powder, and (2) a 25-50 μm thick top layer of coating material. The substrate powder additions were made to improve coating adhesion and minimize differences in coefficient of thermal expansion (CTE) between the coating and substrate. Multiple component coatings were produced by blending the constituent compound powders prior to VPS deposition. Two commercially available alumina - titanium dioxide (Al_2O_3-TiO_2) coatings were deposited on molybdenum and niobium substrates by Praxair Surface Technologies, Indianapolis, Indiana (Table I). While the exact ratio of Al_2O_3 to TiO_2 is proprietary, the coating compositions were produced by blending pure compound powders prior to deposition. Coatings 25-50 μm thick were applied by VPS, while coatings 25-50 μm and 125-175 μm thick were applied by a detonation gun (D-gun) technique.

Amorphous SiO_2 coatings with dispersed carbon particulates were obtained from Illinois Institute of Technology (IIT) Research Institute, Chicago, Illinois (Table I) [1]. These coatings were applied using two different binders (silicate and silicone) at three thicknesses (50, 100, and 150 μm) on molybdenum and niobium substrates. These coatings are applied as a slurry and then fused by a high temperature curing process (dip + fuse process).

Molybdenum and niobium substrates were arc textured using carbon or SiC electrodes at NASA Lewis Research Center (NASA-LeRC), Cleveland, Ohio, by sweeping an electric arc between a carbon or SiC electrode and the specimen surface in an argon atmosphere [2]. Molybdenum coupons were textured at NASA-LeRC using an electron cyclotron resonance atomic oxygen (AO) beam source [3] while holding the substrates at two different temperatures (1100°C or 1300°C) for 102 minutes. The intent was to use a directed AO beam to produce volatile Mo-oxides that subsequently evaporate at high temperature and leave a rough surface with high emittance. Laser ablation is another surface texturing method used to produce Laser Induced Micro-roughened structures (LIMS) with roughness features on the scale of 0.25 to 300 μm in depth and peak to peak dimension by multiple, focused, pulsed beams from high power inert/halide gas lasers [4,5]. Niobium, molybdenum, and Haynes 230 substrates were processed using laser ablation in air or inert argon atmosphere using various pulses/unit-area and laser pulse energy. CVD rhenium whiskers deposited on molybdenum substrates were produced by Ultramet Inc., Pocoima, CA.

The as-received and post-anneal surfaces of coated/surface modified coupons were characterized using Scanning Electron Microscopy (SEM), X-ray Diffraction (XRD), and metallography. Total (wavelength = 0.25 to 15 μm) hemispherical (solid angle approximately equal to 2π) emittance of the pre- and post-anneal coupons were

determined at NASA-LeRC by measuring spectral reflectance at low temperature (82°C) with the assumption of no transmittance (emittance = 1 - reflectance) [6]. The spectral emittance at 82°C is assumed to be an approximate measure of the total hemispherical emittance at high temperatures with the assumption that the optical properties of the material are independent of temperatures [6]. The total hemispherical emittance at a given temperature ($\epsilon(T_A)$) is calculated from the spectral emittance data and the black body distribution function at the temperature of interest

$$\epsilon(T_A) = \frac{\int_{0.25\mu m}^{15\mu m} \epsilon_\lambda(\lambda,T_A)\ \epsilon_{\lambda b}(\lambda,T_A)\ d\lambda}{\sigma T_A^4} \qquad (1)$$

where ϵ_λ is the spectral emittance at a wavelength λ, $\epsilon_{\lambda b}$ is the blackbody emittance at a wavelength λ, σ is the Stefan Boltzmann constant, and T_A is the temperature of interest [7].

The thermal stability of the coatings/surface modifications was evaluated by a dynamic vacuum (< 10^{-5} torr) anneal at 1100°C for 500 hours. The same coupon was used for the pre- and post-anneal emittance measurements. Thermal cycling was accomplished by heating at 2000°C/hour to 1100°C in vacuum (< 10^{-5} torr), holding for 10 minutes, and then quenching with ultra-high purity helium to produce an average cooling rate of about 3500°C/hour between 1100° and 350°C. Ten thermal cycles were completed for a preliminary evaluation.

3. Results for Coated Substrates

The measured emittance values for uncoated molybdenum, niobium, and Haynes 230 were low, as anticipated (Table I). The formation of a thin surface oxide that remains on the surface after vacuum annealing likely results in a higher post-anneal emittance. However, the post-anneal emittance values were all less than 0.70.

Pre- and post-anneal emittance measurements for eleven VPS coatings are given in Table I. The emittance values of four VPS coatings (TiC, TiC + 5% Al_2O_3 + 5% TiO_2, ZrB_2, and ZrB_2 + 10% $MoSi_2$) were all below a value of 0.8. These four VPS coatings were observed to contain some substrate powder at the coupon surface, which have little influence on the emittance values. The low emittance of these four coatings likely results from the inherently low emissivity of the major constituents, TiC and ZrB_2 [8]. Although the as-received emittance values for VPS Cr_2O_3 coatings were fairly high, significant weight loss (0.26 to 17.91 mg/cm^2), coating volatilization, and a decrease in emissivity were observed after vacuum annealing. Cr_2O_3 is known to exhibit high vapor pressures in vacuum at temperatures above 900°C [8]. Even though the Cr_2O_3 coating was observed to contain substrate powder particles and oxides (Mo-oxide, Nb-oxide, and Ni-oxide), this Cr_2O_3 coating exhibits an unacceptable level of volatility.

Six of the eleven VPS coatings (ZrO_2 + 18% TiO_2 + 10% Y_2O_3, ZrC, Fe_2TiO_5, $ZrTiO_4$, ZrO_2 + 8% Y_2O_3 + 2% HfO_2, and Al_2O_3-TiO_2) exhibited pre- and post-anneal emittance values that were close to or above a value of 0.8, see Table I. Emissivity values determined for the TiC, ZrB_2, and ZrC coatings are close to the range of emissivity values reported in the literature for bulk TiC (0.65 to 0.72), ZrB_2 (0.45 to 0.80), and ZrC (0.45 to 0.80) prepared by various processing methods [9]. The emissivity values in Table I are a reasonable match to values previously measured for thermal spray coatings of Fe_2TiO_5 (0.88 to 0.85), $ZrTiO_4$ (0.88 to 0.86), and Al_2O_3-12%TiO_2 (0.87 to 0.86) deposited on Nb-1Zr [10]. Thus, although the emissivity values are not measured at temperature, the extrapolated data appears to be a reasonable estimate of high-temperature emittance [6,7].

Pre-anneal emittance data for most of the VPS coatings are generally independent of substrate, but the post-anneal emissivity results are generally dependent on substrate type (Table I). Small decreases in emissivity were observed after annealing for the ZrC coating deposited on molybdenum and niobium, while a large decrease was observed for the ZrC coating deposited on Haynes 230. SEM and XRD examinations of the as-received coupons indicate that the coating is ZrC, but substrate particles were detected at the coating surface (Figure 1) and ZrO_2 was present from ZrC oxidation. These surface particles may be substrate powder from the bond layer that was kicked up into the top layer of the coating during the VPS deposition process, or powder added intentionally to the coating deposit for improved adhesion. Figure 1b shows that there was little interaction between the niobium substrate particles and the ZrC coatings after vacuum annealing, and the small change in weight (0.096 mg/cm^2) indicates that the ZrC coating deposited on niobium was very stable. The small decrease in post-anneal emissivity (Table I) with no observed change in coating composition indicates that the ZrC coating deposited on molybdenum was also very stable. A higher density of base metal powder particles was observed in the ZrC coating deposited on Haynes 230, and SEM analysis detected elements not associated with Haynes 230 (niobium, molybdenum, sulfur, titanium, and calcium). A significant amount of weight loss (21.91 mg/cm^2) and reactive interaction between the Haynes 230 substrate particles and the ZrC coating was observed after vacuum annealing (Figure 2) with coating porosity being observed. The reaction between the ZrC coating and the Haynes 230 substrate particles likely produces the large decrease in post-anneal emissivity (Table I). Uncoated Haynes 230 exhibits a larger weight loss (24.61 mg/cm^2) from vacuum annealing as a result of chromium-oxide formation and evaporation [8]. Examination of Table I indicates that the inherent volatility of Haynes 230 generally resulted in a significantly different post-anneal emittance value than measured for the coated molybdenum and niobium substrates.

Substrate metal particles were also detected at a lower density on the surface of Fe_2TiO_5 and $ZrTiO_4$ coatings using SEM and XRD. Only a small decrease in post-anneal emissivity was observed for Fe_2TiO_5 deposited on molybdenum, while a larger decrease in post-anneal emissivity was observed for Fe_2TiO_5 coatings deposited on niobium. Post-anneal spalling is observed for the Fe_2TiO_5 and $ZrTiO_4$ coatings deposited on Haynes 230, which was likely produced by coating reaction between the substrate or Haynes 230 substrate powder in the coating. In all cases for the Fe_2TiO_5 coatings, a loss of iron-oxide was detected in the post-anneal SEM analysis. The equilibrium partial pressure for FeO vapor was calculated to be on the order of 10^{-5} atmospheres in a vacuum of the order of 10^{-6} torr, which indicates that some loss of iron-oxide would be expected during the 1100°C vacuum anneal [10]. The loss of iron-oxide may contribute to the lower post-anneal emittance values for the Fe_2TiO_5 coating deposited on niobium and Haynes 230. The reported normal emittance values for Nb_2O_5 is less than Fe_2TiO_5 [8], which indicates that conversion of the substrate particles into Nb-oxides during vacuum annealing would reduce the emissivity of the Fe_2TiO_5 coating. The fairly significant decrease in post-anneal emittance was the same for the $ZrTiO_4$ coatings deposited on molybdenum and niobium. XRD analysis indicated that the $ZrTiO_4$ coating contained a high fraction of ZrO_2 and TiO_2 in addition to $ZrTiO_4$. Little change in the $ZrTiO_4$ coating composition deposited on niobium was observed after vacuum annealing (Table 4.9), which indicates that oxidation of the niobium substrate particles during vacuum annealing could decrease the emissivity. Molybdenum substrate particles were lost from the $ZrTiO_4$ coating deposited on molybdenum after vacuum annealing, which indicates that oxidation of the molybdenum substrate particles and Mo-oxide evaporation may decrease the post-anneal emittance. Reducing the substrate powder content could improve the post-anneal emittance and stability of the Fe_2TiO_5 and $ZrTiO_4$ coatings.

Little change in emissivity was observed for the ZrO_2 + 18% TiO_2 + 10% Y_2O_3, ZrO_2 + 8% Y_2O_3 + 2% HfO_2, and Al_2O_3-TiO_2 coatings after annealing, and the post-anneal emittance values were independent of substrate (Table I). Little or no substrate powder was detected on the surfaces of these coated coupons. Minimizing the substrate powder content of the coatings and the high stability of these oxide coatings (ZrO_2 + 18% TiO_2 + 10% Y_2O_3, ZrO_2 + 8% Y_2O_3 + 2% HfO_2, and Al_2O_3-TiO_2) results in little change in emittance, weight change (0.1 to 0.5 mg), or coating composition with annealing. The as-deposited emittance values for the Al_2O_3-TiO_2 coatings deposited by D-gun were slightly higher than the VPS coatings, but the post-anneal emittance values were equivalent. The VPS Al_2O_3-TiO_2 coatings (Figure 3a) were observed to have a smoother surface, slightly higher TiO_2 content (11 to 20 atomic% titanium versus 10 to 12 atomic% titanium for the D-gun coating), coarser two-

phase structure, and slightly different phases detected by XRD (TiO_2(rutile), α-Al_2O_3, and γ-Al_2O_3 for VPS versus TiO_2(rutile), χ-Al_2O_3, and γ-Al_2O_3 for D-gun). The finer initial particle size and higher energy deposition used in the D-gun process produces the finer phase structure and rougher surface, see Figure 3b. Post-anneal XRD indicated that all the rutile had converted to $Al_2Ti_7O_{15}$ and only the α-Al_2O_3 polymorph was present for both the VPS and D-gun Al_2O_3-TiO_2 coatings. The similarity in phase composition likely results in comparable post-anneal emittance values for the Al_2O_3-TiO_2 coatings deposited by VPS or D-gun.

SEM/EDS and XRD characterization indicates that the dip + fuse (SiO_2 + C) coatings are amorphous and contain only silicon, carbon, and oxygen. Although the emittance values for the as-deposited dip + fuse (SiO_2 + C) coatings were very high, significant decreases in emissivity, weight loss (1.66 to 5.97 mg/cm^2), and coating disintegration were observed after vacuum annealing (Table I). The dip + fuse (SiO_2 + C) coatings were also observed to spall after a few thermal cycles, which indicates there was a large CTE difference between the coating/substrate. The use of a silicon or silicate binder to produce the dip + fuse coatings did not change the results. SiO_2 is known to exhibit high vapor pressures at low oxygen partial pressures [8], and the results were not changed by the presence of carbon in the coatings. Thus, the dip + fuse (SiO_2 + C) coatings do not have the needed stability in vacuum at high temperature.

The as-received emittance values for the carbon and SiC electrode arc textured coupons were high and independent of the molybdenum or niobium substrate, but a significant decrease in emissivity was observed after annealing, see Table II. The emittance values of carbon (graphite) and SiC materials are fairly high [9], and high emittance values for the as-received coatings are expected. However, the carbon and SiC electrode arc textured deposits were fairly thin (10-20 μm). The rates of carbon and SiC interdiffusion with molybdenum and niobium are high enough at 1100°C for the deposits to be consumed by inward diffusion of carbon and silicon into the substrate with limited formation of carbide and silicide compounds that have low emittance [11,12]. The high rates of coating/substrate interdiffusion result in a low post-anneal emissivity.

4. Results for Surface Texturing

Figure 4 shows that the high aspect ratio (H/D>5) rhenium whiskers produced by CVD. As-received emittance values for the best CVD rhenium coatings are above a value of 0.8, see Table II. The 30 and 75 minute CVD runs produced average whisker heights of about 12 μm and 30 μm, which indicates that a 75 minute deposition time is required to produce the high aspect ratio whiskers for a higher as-received emissivity. The 90 minute run

produced a higher density of rhenium whiskers, but the deposit was less adherent and hot isostatically pressing (HIP) at 20 ksi and 1200°C for 2 hours was required to prevent delamination of the coating during cutting operations. The HIP treatment appears to have smoothed and slightly densified the rhenium whiskers produced by the 90 minute run. Comparison of the emittance data for the 30, 75, and 90 minute CVD runs in Table II indicates that there is some effect of whisker density versus perceived black body area created by the high aspect ratio whiskers, and the deposit produced by the 75 minute run provided optimum results.

The post-anneal emittance value for the CVD rhenium whisker deposit produced by the 90 minute run was significantly less than in the as-received condition. Since the 90 minute run with post-deposition HIP produces a more closely spaced distribution of rhenium whiskers, surface diffusion during annealing would be expected to more easily result in surface smoothing with a corresponding decrease in emissivity. The low weight loss for the CVD rhenium whisker coated coupon (0.052 mg/cm^2) could result from some limited oxidation/evaporation during the vacuum annealing, but this minor surface oxidation likely had less influence on the post-anneal emittance than the coarsening of the whiskers. The CVD rhenium whiskers produced by the 75 minute run in Figure 4 are more widely spaced, and are expected to exhibit more resistance to smoothing from surface diffusion during vacuum annealing to give higher post-anneal emittance values.

The substrate temperatures used for AO beam texturing (1100°C and 1300°) of molybdenum were well above the temperature at which the oxides of molybdenum (MoO_2 and MoO_3) are volatile (~600°C) [8]. SEM examination showed that the surfaces were only slightly roughened by the AO beam texturing process, and the emissivity of the 1100°C AO textured surface (Table II) was only slightly higher than flat molybdenum. The 1300°C AO beam textured surface had a much higher as-received emittance value, but SEM examinations revealed that the surface was covered with Mo-oxide. The low post-anneal emittance value for the 1300°C AO beam texture surface results from the evaporation of the Mo-oxides. Since high aspect ratio surface roughening was not produced by the AO beam texturing process, the post-anneal emittance values are low and similar to that of the starting molybdenum substrate.

The as-received emissivity values for the molybdenum, niobium, and Haynes 230 coupons that were textured in air using laser ablation or LIMS are generally fairly high (Table II), but the post-anneal emissivity values were comparable to the respective uncoated substrates (Table I). The as-received emittance values for the coupons that were LIMS textured in argon were low as a surface oxide was not formed, and the post-anneal values were

comparable to the respective uncoated substrates, see Tables I and II. SEM examinations of the as-received LIMS textured surfaces showed that the surfaces were only slightly roughened, and covered with an oxide. The surface oxide on the coupons LIMS textured in air produces the higher as-received emittance values, but the oxide is removed by either evaporation (molybdenum and Haynes 230) or base metal interdiffusion during vacuum annealing. Since LIMS texturing resulted in only surface roughening with limited surface oxidation rather than high aspect ratio whiskers, many of the pre-anneal emittance values and all of the post-anneal emittance values for the LIMS textured molybdenum, niobium, and Haynes 230 substrates were low.

5. Thermal Cycle Testing

The six VPS coatings (ZrO_2 + 18% TiO_2 + 10% Y_2O_3, ZrC, Fe_2TiO_5, $ZrTiO_4$, ZrO_2 + 8% Y_2O_3 + 2% HfO_2, and Al_2O_3-TiO_2 (both VPS and D-gun)) and CVD rhenium whisker coating were subjected to ten thermal cycles in vacuum. Following ten thermal cycles the VPS and D-gun coatings deposited on molybdenum and niobium substrates had a low weight change (-0.086 to 0.034 mg/cm^2) that was comparable to the uncoated controls (-0.009 to 0.009 mg/cm^2), and no spalling was observed. Bare Haynes 230 (-0.26 mg/cm^2) and the coated Haynes 230 coupons (-0.12 to -0.050 mg/cm^2) exhibited a higher weight loss due to high-temperature evaporation from the Haynes 230 substrate in vacuum, as observed in vacuum annealing. The Fe_2TiO_5 and $ZrTiO_4$ coating deposited on Haynes 230 exhibited a high weight loss (-0.22 to -0.050 mg/cm^2) and spalling after thermal cycling. Coating/substrate interactions and CTE differences between the Fe_2TiO_5 or $ZrTiO_4$ coatings and the Haynes 230 base material likely produce this spalling. A fairly high weight loss (-0.23 mg/cm^2) was initially observed for the CVD rhenium whisker coating after the first thermal cycle, but no additional change in weight or coating deadhesion was observed at the end of the ten thermal cycles. The high initial weight loss was probably produced by the evaporation of surface contamination or oxide entrapped in the CVD rhenium whiskers. These results indicate that most of the coatings are resistant to thermal cycling.

6. Summary

VPS coatings, Al_2O_3-TiO_2 D-gun coatings, dip + fuse (SiO_2 + C) coatings, carbon and SiC electrode arc texturing, AO beam texturing, LIMS surface texturing, and CVD rhenium whisker coating were evaluated to increase the surface emissivity of molybdenum, niobium, and Haynes 230. The stability and durability of these coatings was evaluated by an 1100°C/500h anneal in vacuum and thermal cycling in vacuum.

As summarized in Tables I and II, many of the coatings/surface modifications evaluated are not desirable due to a low as-received emissivity (VPS TiC, TiC + 5% Al_2O_3 + 5% TiO_2, ZrB_2, and ZrB_2 + 10% $MoSi_2$ coatings; AO beam texturing and LIMS surface texturing) or low post-anneal emittance due to coating/substrate interdiffusion (carbon and SiC electrode arc texturing), coating volatilization (VPS Cr_2O_3 coating, and dip + fuse (SiO_2 + C) coatings), or stability (AO beam texturing, and LIMS). However, six plasma spray coatings (ZrO_2 + 18% TiO_2 + 10% Y_2O_3, ZrC, Fe_2TiO_5, $ZrTiO_4$, ZrO_2 + 8% Y_2O_3 + 2% HfO_2, and Al_2O_3-TiO_2 (both VPS and D-gun)) and a CVD rhenium whisker coating did have pre- and post-anneal emittance values that were higher than or close to a value of 0.8. These coatings generally exhibited favorable stability during vacuum annealing, and excellent resistance to thermal cycling. These coatings could be used on TPV radiator surfaces to improve the surface emittance of molybdenum, niobium, or nickel base metals with minimal lifetime degradation.

Acknowledgments

This work was performed under USDOE Contracts. DE-AC11-93PN38195 and DE-AC11-98PN38206. The technical comments and contributions of R. Bianco, J. L. Hollenbeck, W.L. Ohlinger, D.P. Measures, and J.J. Yue are appreciated.

References

[1] Y. Harada and R.J. Mell, Proceedings of SPIE - The International Society for Optical Engineering, 1330 (1990) 90.

[2] B.A. Banks, S.K. Rutledge, M.J. Mirtich, T. Behrend, D.L. Hotes, M.T. Kussmaul, C. Stidham, T. Stueber. J. Barry, and F. DiFilippo, Arc-Textured Metal Surfaces for High Thermal Emittance Space Radiators, NASA-TM-100894, 1988.

[3] S.K. Rutledge, D.L. Hotes, and P.E. Paulsen, The Effects of Atomic Oxygen on the Thermal Emittance of High Temperature Radiator Surfaces, NASA-TM-103224, 1989.

[4] R.K. Singh, Method of Applying a Laser Beam Creating Micro-scale Surface Structures Prior to Deposition of Film for Increased Adhesion, U.S. Patent 5,558,789, September 24, 1996.

[5] R.K. Singh, S. Behl, and D. Bhattacharya, Method of Increasing the Surface Area of Ceramics, Metals, and Composites, U.S. Patent 5,473,138, December 5, 1995.

[6] S.K. Rutledge, M.J. Forkapa, and J.M. Cooper, Thermal Emittance Enhancement of Graphite-Copper Composites for High Temperature Space Based Radiators, NASA-TM-105178, 1991.

[7] M.J. Mirtich, and M.T. Kussmaul, Enhanced Thermal Emittance of Space Radiators by Ion Discharge Chamber Texturing, NASA-TM-100137, 1987.

[8] P. Kofstad, High Temperature Corrosion, Elsevier, New York, 1988.

[9] Y.S. Touloukian and D.P. Dewitt, Thermal Radiative Properties of Nonmetallic solids, Thermophysical Properties of Matter: Volume 8, IFI/Plenum, New York, 1972.

[10] R.E. Cleary, R. Emanuelson, W. Luoma, and C. Ammann, Properties of High Emittance Materials, NASA-CR-1278, 1969.

[11] K. Kurokawa and R. Nagasaki, Proc. Int. Symp. & Exhibit on Sci. And Technol. Of Sintering, Tokyo, (1987), 1397.

[12] M. Naka, T. Saito, and I. Okamoto, J. Mat. Sci., 26 (1991) 1983.

Table I: Emissivity values measured at room temperature and extrapolated to 1100°C for candidate coatings deposited by a VPS, D-gun, or dip + fuse process. As-coated and post-anneal measurements were made on the same coupon. Data for uncoated substrates are included for comparison.

Coating Composition / Deposition Method	Hemispherical, Total Emissivity at 1100°C; Molybdenum substrate		Hemispherical, Total Emissivity at 1100°C; Niobium substrate		Hemispherical, Total Emissivity at 1100°C; Haynes 230 substrate		Comments
	As-coated	Annealed	As-coated	Annealed	As-coated	Annealed	
Uncoated Substrates	0.12 to 0.14	0.26	0.12	0.54	0.23	0.67	
ZrC / VPS	0.91	0.86	0.89	0.85	0.89	0.72	
TiC / VPS	0.75	0.54	0.75	0.50	0.78	0.71	Low emissivity
Fe_2TiO_5 / VPS	0.90	0.89	0.92	0.73	0.89	0.75	
$ZrTiO_4$ / VPS	0.88	0.75	0.85	0.77	0.89	0.85	
ZrO_2 + 18% TiO_2 + 10% Y_2O_3 / VPS	0.86	0.85	0.86	0.85	0.88	0.85	
ZrO_2 + 8% Y_2O_3 + 2% HfO_2 / VPS	0.75	0.69	0.82	0.78	0.79	0.85	
ZrB_2 / VPS	0.72	0.60	0.71	0.51	0.82	0.53	Low emissivity
ZrB_2 + 10% $MoSi_2$ / VPS	0.75	0.59	0.75	0.67	--	--	Low emissivity
Cr_2O_3 / VPS	0.90	0.78	0.90	0.59	0.89	0.81	Poor stability
TiC + 5% Al_2O_3 + 5% TiO_2 / VPS	0.77	0.56	0.79	0.62	0.79	0.63	Low emissivity
Al_2O_3-TiO_2 / VPS	0.88	0.88	0.88	0.87	--	--	
Al_2O_3-TiO_2 (25-50 μm) / D-gun	0.93	0.87	0.93	0.85	--	--	
Al_2O_3-TiO_2 (125-175 μm) / D-gun	0.96	0.90	0.95	0.90	--	--	
Silicone Binder (50 μm) / dip + fuse	0.95	0.57	0.95	0.83	--	--	Poor stability
Silicone Binder (150 μm) / dip + fuse	0.97	0.86	0.97	0.88	--	--	Poor stability
Silicate Binder (50 μm) / dip + fuse	0.94	--	0.95	--	--	--	Poor stability
Silicate Binder (150 μm) / dip + fuse	0.95	--	0.95	--	--	--	Poor stability

Table II: Emissivity values measured at room temperature and extrapolated to 1100°C
for candidate coatings deposited by arc texturing (AT),
and surface modifications produced by atomic oxygen texturing (AOT),
laser Texturing (LIMS), or CVD rhenium whisker deposits.
As-received and post-anneal measurements were made on the same coupon.

Coating Composition / Deposition Method	Hemispherical, Total Emissivity at 1100°C; Molybdenum substrate		Hemispherical, Total Emissivity at 1100°C; Niobium substrate		Hemispherical, Total Emissivity at 1100°C; Haynes 230 substrate		Comments
	As-received	Annealed	As-received	Annealed	As-received	Annealed	
Carbon electrode / AT	0.90	0.26	0.90	0.54	--	--	Poor stability
SiC electrode / AT	0.92	0.33	0.92	0.46	--	--	Poor stability
CVD rhenium (30 minute run)	0.75	--	--	--	--	--	
CVD rhenium (75 minute run)	0.85	--	--	--	--	--	
CVD rhenium (90 minute run)	0.80	0.70	--	--	--	--	
AOT at 1100°C	0.80	0.08	--	--	--	--	Poor stability
AOT at 1300°C	0.15	0.10	--	--	--	--	Low emissivity
LIMS in air	0.96 to 0.45	0.20 to 0.17	0.94 to 0.78	0.26 to 0.10	0.94 to 0.68	0.68 to 0.66	Poor stability; Low emissivity
LIMS in argon	0.45	0.11	0.77	0.10	0.70	0.76	

(a)

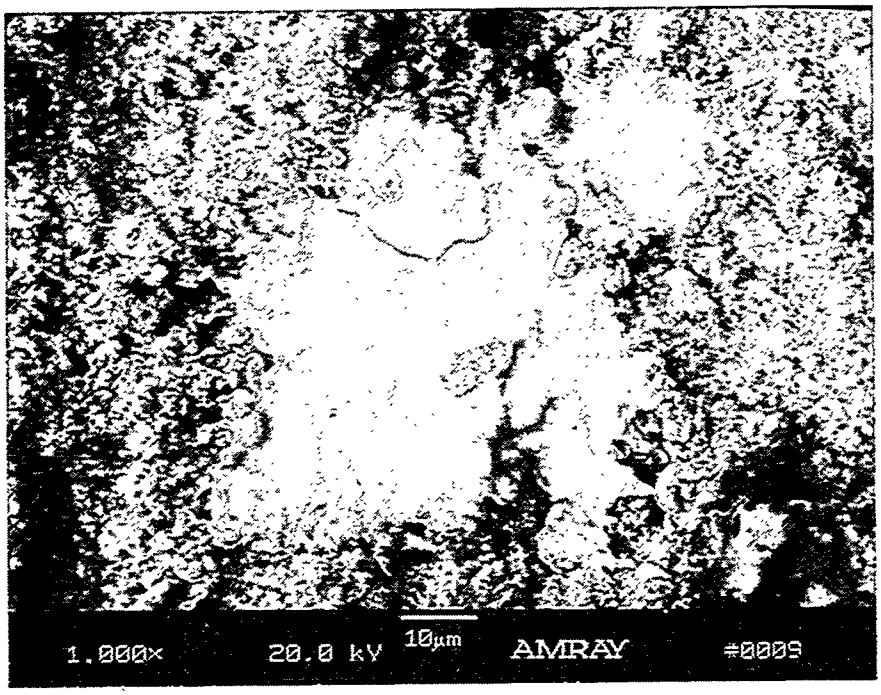

(b)

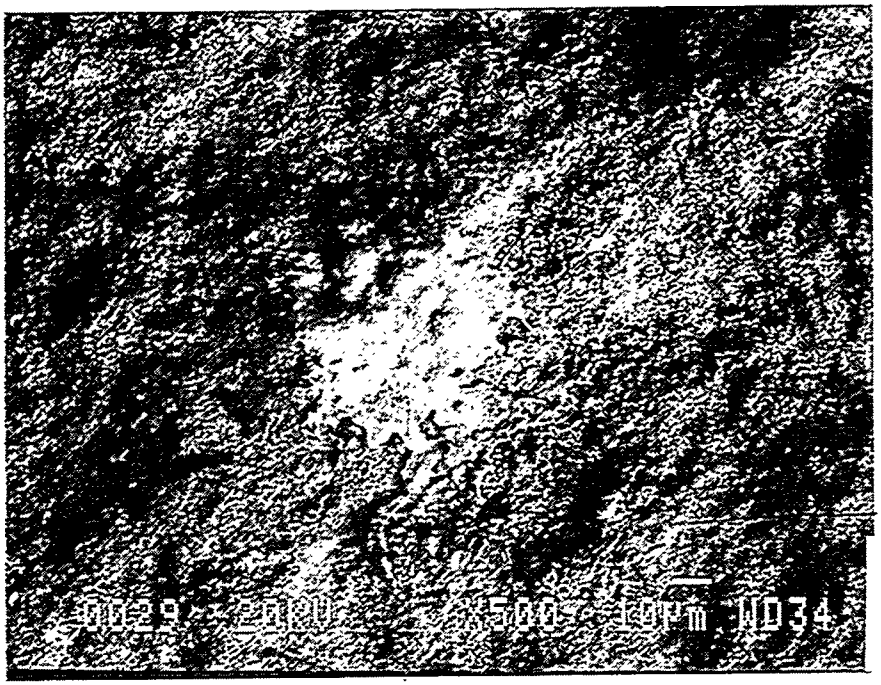

Fig. 1. SEM / back-scattered electron (BSE) examination of the surface of a VPS ZrC coating deposited on niobium: (a) as-coated surface showing a niobium-rich substrate particle on the coating surface (magnification = 1000X), and (b) coating surface after vacuum annealing showing a niobium-rich particle at 500X magnification.

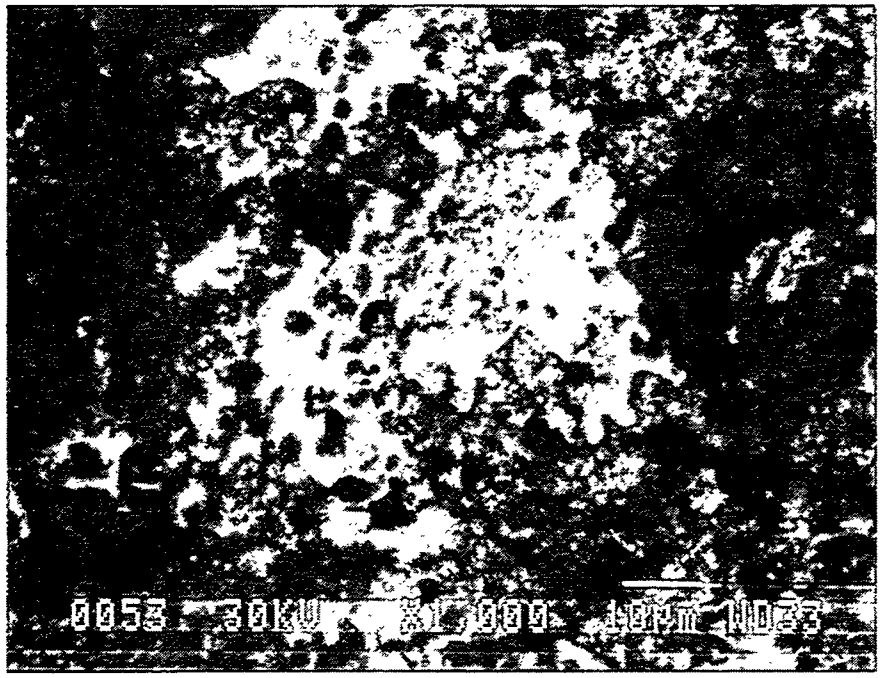

Fig. 2. SEM/BSE examination of surface of a VPS ZrC coating deposited on Haynes 230 after vacuum annealing showing the reactive interaction between the coating and a base metal particle (magnification = 1.000X).

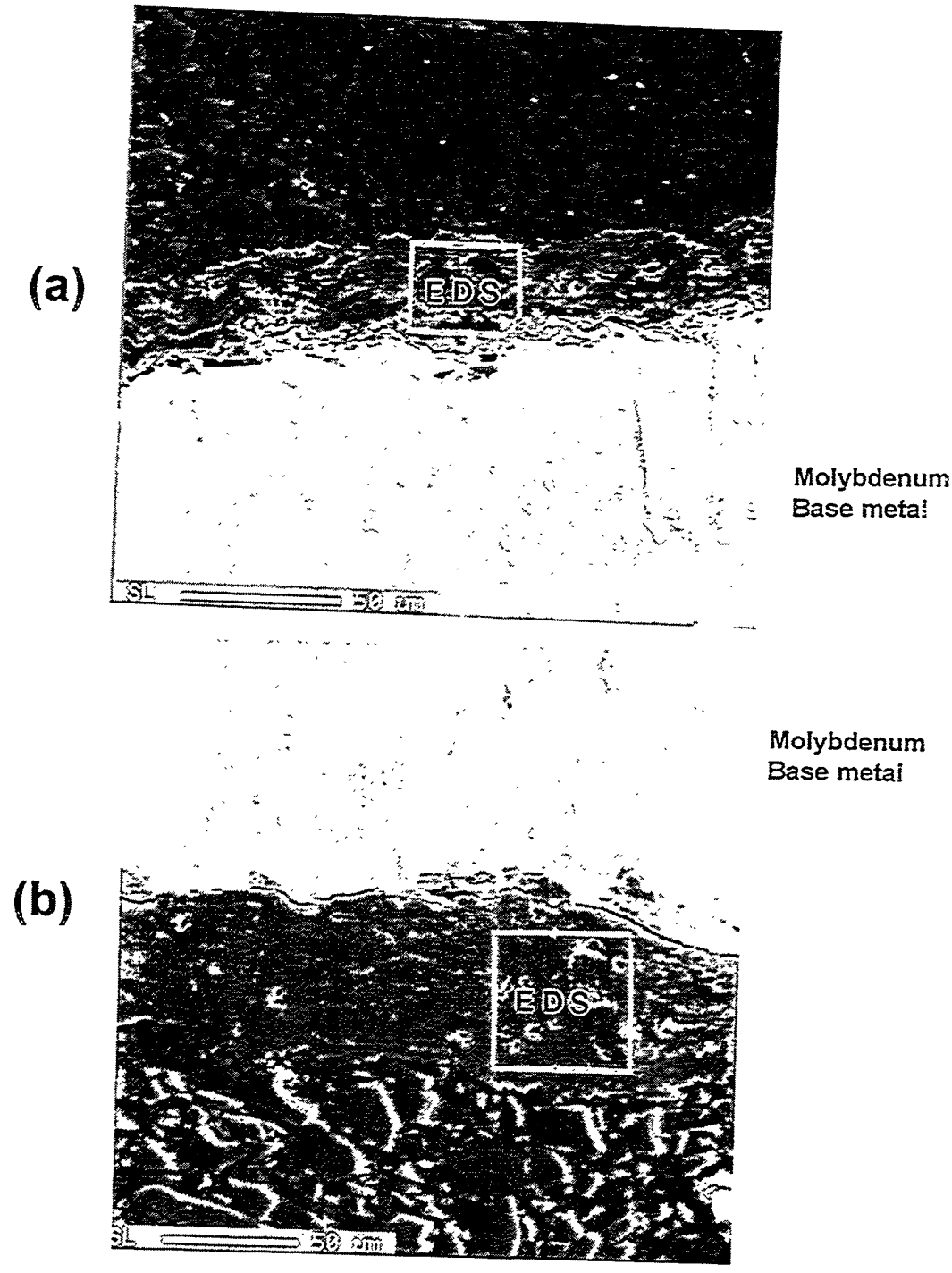

Fig. 3. SEM/BSE examination of the cross-section of as received Al_2O_3-TiO_2 coatings: (a) 25 - 50 μm thick coating deposited by VPS on molybdenum (Mag=500X), and (b) 125 to 175 μm thick coating deposited by D-gun on molybdenum (Mag=500X).

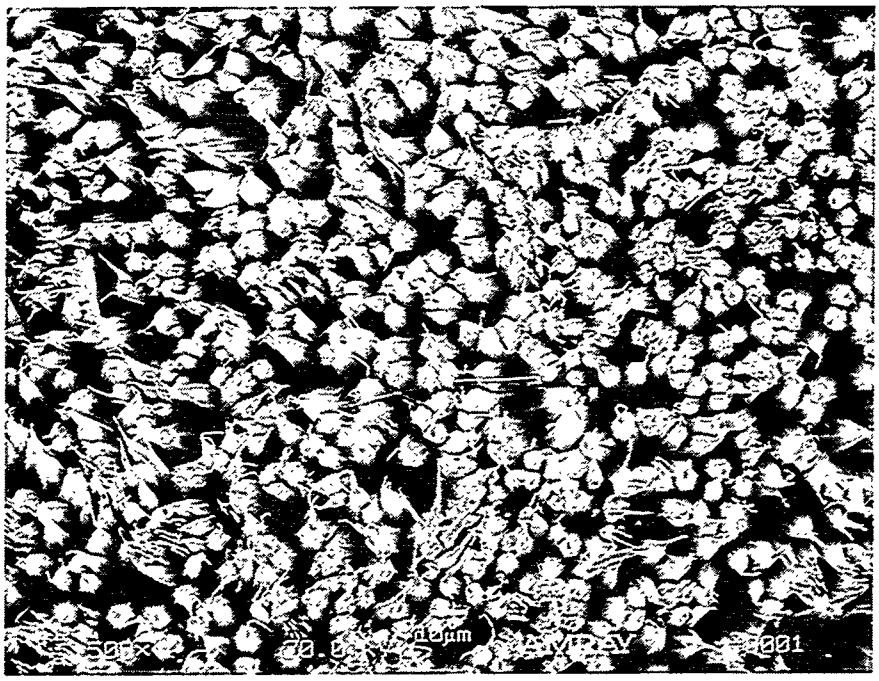

Fig. 4. SEM/SE examination of the as-received surface of CVD rhenium whisker coating produced by a 75 minute deposition run (Mag=500X). The coating was deposited on molybdenum.